pISSN 1229-3008 eISSN 2287-6251
Progress in Superconductivity and Cryogenics
Vol.21, No.2, (2019), pp.45~49 https://doi.org/10.9714/psac.2019.21.2.045

Comparison between analytic and numerical approaches to calculate screening current induced field in HTS magnet

Jeseok Bang[a], Seokho Kim[b], Jaemin Kim[a], Soobin An[a], Chaemin Im[a], and Seungyong Hahn[*,a]

[a] *Seoul National University, Seoul, Korea*
[b] *Changwon National University, Changwon, Korea*

(Received 21 February 2019; revised or reviewed 25 May 2019; accepted 26 May 2019)

Abstract

This paper reports comparison between analytic and numerical simulation approaches for calculation of screening current and screening current induced field in a high temperature superconductor magnet. Bean slab model is adopted to calculate screening current and SCF analytically, while the finite element method numerically. A case study of screening current and SCF calculation are conducted with a magnet, a 7 T 68 mm cold-bore multi-width no-insulation GdBCO magnet built and tested by Massachusetts Institute of Technology Francis Bitter Magnet Laboratory. In this study, we assume the magnet is dunked in liquid nitrogen at 77 K. Furthermore, the simulation results are compared in terms of computation time and accuracy. Finally, discussion on the different methods together with the comparison between the calculations and experiment is provided.

Keywords: HTS magnet, screening current induced field, screening current, bean slab model, edge-element, domain homogenization

1. INTRODUCTION

This paper presents simulation approaches to calculate screening current and screening current induced field (SCF) in a high temperature superconductor (HTS) magnet. Unlike a resistive magnet, screening current is induced in an HTS magnet without being dissipated, and it is well-known that its magnitude is proportional to that of radial magnetic field, which is penetrating component against an HTS tape width. Screening current, a major source of SCF, is of importance for magnet analysis because it causes performance degradation such as generated magnetic field degradation, field homogeneity distortion, and other negative effects [1, 2]. Because of this importance, research on screening current and SCF has been conducted with many experiments [3-7], and calculation method of screening current and SCF have been developed with multiple studies [8-26]. As a result, two methods, an analytic method [8-12] and a numerical method [13-26], have been proposed. Despite these developments, a comparison between analytic and numerical methods has not been discussed sufficiently. Thus, this paper suggests a typical simulation approach of each method and evaluates the approaches with a case study of a 7 T 68 mm cold-bore multi-width no-insulation GdBCO magnet in liquid nitrogen cooled environment of 77 K which was constructed and tested by the MIT Francis Bitter Magnet Laboratory [27]. For a precise analysis of the magnet, screening current and the measured magnet dimensions are considered; they are well-known major sources of large discrepancy between calculated and measured magnetic field. Finally, discussion on not only simulation results with each approach but also the difference between calculation and measurement would be provided.

* Corresponding author: hahnsy@snu.ac.kr

2. SIMULATION APPROACHES

2.1. Bean Slab Model

Bean slab model is a typical approach of an analytic method [28]. Fig. 1(a) indicates a current density of transport current and a magnetic field inside a slab without an external field which is called virgin state, while Fig. 1(b) with an external field. The particular current density and the magnetic field inside a slab are classified depending on the magnitude of an external magnetic field and a critical current density. Firstly, the field configuration is equal to Fig. 2 (a) when the intensity of external field (H_e) is less than that of the virgin state field (H_v). Secondly, the field configuration is equal to Fig. 2 (b) when H_e is more than H_v and less than twice of H_v. Lastly, the field configuration is identical to Fig. 2 (c) when H_e is more than twice of H_v. These classifications are applied to simulate screening current. For simulation of screening current and SCF with this model, magnetic field calculation is firstly performed at the center of all individual turns assuming that an operating current flows uniformly in each single pancake (SP) in an HTS magnet; in this process, Gaussian quadrature and elliptic integral should be used to calculate the field. With the calculation results, a critical current density of a slab, an inclination of the graphs in Fig. 2, is determined based on measured critical current $I_c(|B|, \theta)$ data. Finally, a penetration depth, which is an important

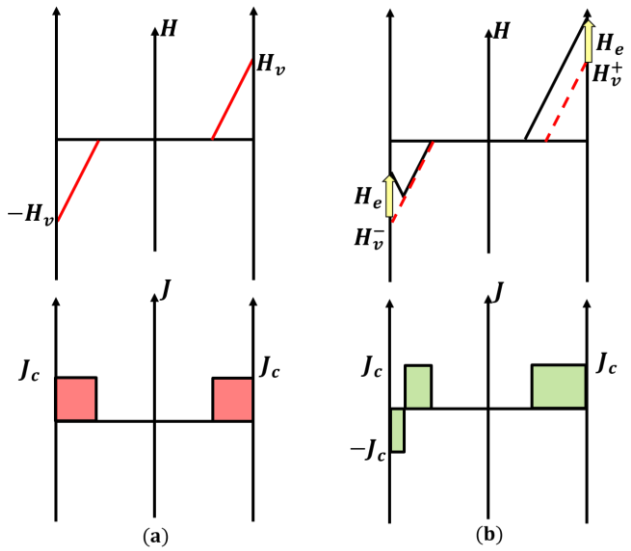

Fig. 1. Bean slab model: (a) virgin state; (b) exposed to an external magnetic field. Dash lines shown in (b) is equal to the field (H) graph in (a). The x-axis indicates the width of an HTS tape.

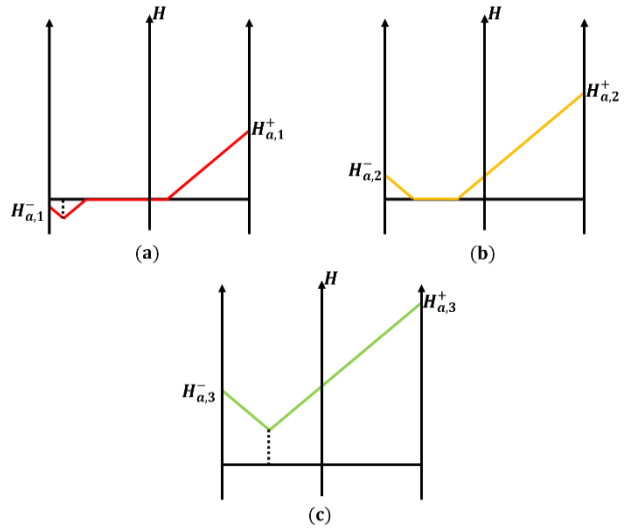

Fig. 2. The three cases of Bean slab model carrying DC transport current; $H_{a,1-3}^{+/-}$ is a boundary field at the edge of an HTS tape. The x-axis indicates the width of an HTS tape.

variable of Bean slab model, is determined with the calculated field and the critical current density [28].

2.2. Finite Element Method

Finite element method (FEM) is a well-known simulation approach of numerical method. In this paper, FEM adopting domain homogenization [29] and H-formulation [30] is described in cylindrical coordinate (r, ϕ, z). Five steps are essentially required to calculate screening current and SCF: 1) selection of a certain basis element; 2) determination of a governing equation; 3) assignment of a boundary condition; 4) assignment of an integral constraint; and 5) consideration of a non-linear material property, index resistivity.

(Step 1) Edge-element or curl element is selected as a basis element of FEM. The element is able to transform conventional second order point form electromagnetics governing equation, vector potential equation, into first-order point form, H-formulation [30]. This transformation is possible since the edge-element satisfies divergence constraints of electromagnetics ($\nabla \cdot \mathbf{H} = 0$ and $\nabla \cdot \mathbf{E} = 0$) in electric charge free space.

(Step 2) Our governing equation is Faraday's law of induction

$$\nabla \times \mathbf{E} = \frac{\partial(\mu_0 \mathbf{H})}{\partial t}, \tag{1}$$

Magnetic field intensity (H), a primary variable, has only radial (H_r) and axial (H_z) components, while electric (E), a secondary variable, azimuthal (E_ϕ).

(Step 3) Boundary condition is equal to a conventional one. When magnetic field simulation is performed with FEM, for example, the region of "air" should be large enough to contain that of "source", and primary field variables are zero at the boundary of the "air". This conventional boundary condition is identically used to calculate of screening current and SCF.

(Step 4) Ampère's circuit law of (2) is used to assign our integral constraint. This circuit law calculates azimuthal current density (J) in an HTS magnet assuming time-varying electric field is almost zero, and an integral of the current density (3) becomes our integral constraint to be satisfied:

$$\nabla \times \mathbf{H} = \mathbf{J} + \frac{\partial \epsilon \mathrm{E}}{\partial t} \approx \mathbf{J}, \tag{2}$$

and

$$\int_S J_\phi(r,z,t)\left(\equiv \frac{\partial H_r}{\partial z} - \frac{\partial H_z}{\partial r}\right) dr dz = I_{op}(t), \tag{3}$$

where $I_{op}(t)$, ϵ and are time-varying operating current, and electric permitivity. Because (3) requires long computation time, (4) was proposed to reduce the time.

$$\int_S J_\phi(r,z,t)\left(\equiv \frac{\partial H_r}{\partial z} - \frac{\partial H_z}{\partial r}\right) dz = \frac{I_{op}(t)}{D}, \tag{4}$$

where D is thickness of an HTS tape. By this development called domain homogenization.

(Step 5) HTS tape has a highly non-linear resistivity [31], index resistivity (ρ), and the resistivity is represented with E-J power law of (5):

$$\rho(J) = \frac{Ec}{Jc}\left|\frac{J}{J_c}\right|^{n-1} = \frac{E}{J}, \tag{5}$$

where J_c, E_c, J, and n stand for, respectively, critical current density, critical electric field of 1 μV/cm, current density, and the index.

3. CASE STUDY: A 7 T 68 MM NO-INSULATION GDBCO MAGNET OPERATING AT 77 K

A case study was conducted with a 7 T 68 mm no-insulation (NI) GdBCO magnet constructed and tested by MIT Francis Bitter Magnet Laboratory [26]; the magnet consists of 13 double pancakes (DPs) wound with GdBCO tape manufactured by SuNAM Co., Ltd. It reached its operating current of 25 A with a certain charging rate of 1 A/min in liquid nitrogen at 77K. Axial magnetic field was measured along the magnet axis within a given range from −40 mm to 40 mm. To carefully conduct the case study, SCF and construction errors of magnet dimensions, such as discrepancy between a designed inner diameter and a measured inner diameter, were taken into account. And, short sample critical current data of SuNAM HTS tape [32], Fig. 3, were provided because of the limit of measured data at 77 K although length-wise critical current data are required for precise calculation of screening current and SCF.

3.1. Key Parameters

Table I shows key parameters for simulation of the magnet. Construction and operation parameters are specified from the reference [27], and the index n is from a reference [32].

3.2. Simulation Results

Fig. 4 shows the simulation results: (a) total current density with assuming current flows uniformly in each single pancake of the HTS magnet ($J_{tot,Ideal}$); (b) total current density with FEM ($J_{tot,FEM}$); (c) total current density with Bean slab model ($J_{tot,Bean}$); (d) screening current density with FEM ($J_{sc,FEM}$); and (e) screening current density with Bean slab model ($J_{sc,Bean}$). Calculation results shown in Fig. 4 (d) and (e) agree reasonably well with a proportional characteristic that the magnitude of screening current is proportional to that of the radial magnetic field. Thus, screening current is intensely induced at top and bottom double pancakes (DPs), while it is marginally induced around the magnet mid-plane.

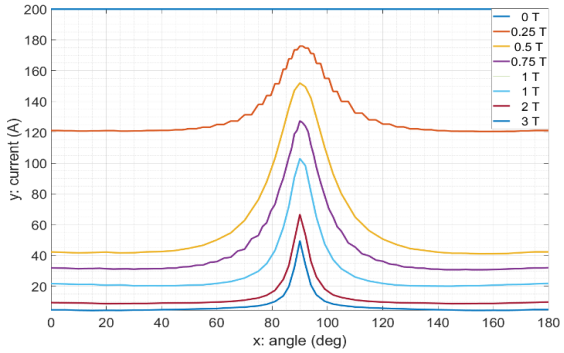

Fig. 3. SuNAM HTS tape critical current (I_c) information measured at 77 K.

TABLE I
KEY PARAMETERS OF THE 7 T 68 MM COLD BORE NI MAGNET.

Construction parameters	Unit	
HTS tape width	[mm]	4.1 - 8.1
Inner diameter (ID)	[mm]	78.0
Outer diameter (OD)	[mm]	101.8
Total height	[mm]	157.7
Operation parameters	Unit	
Operating current, I_{op}	[A]	25
Current chargning rate	[A/min]	1
Operating temperature, T_{op}	[K]	77
Self-field critical current at 77 K, Ic	[A]	200 - 400
Index at 77 K, n	[·]	22

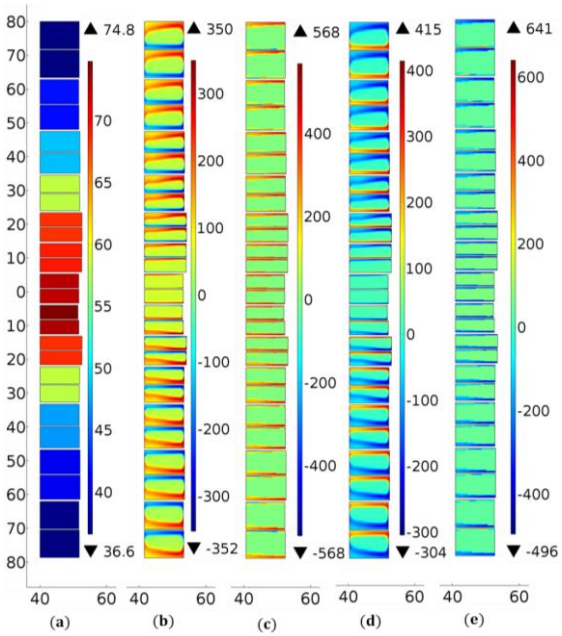

Fig. 4. Simulation results. (a) - (c) stand for total current density, while (d) – (e) screening current density. The y-axis indicates the DP z axis, while the x-axis is for the DP r axis in millimeters. Color bar indicates current density in A/mm^2. The number beside triangles of the color bar indicates the minimum and maximum values.

Fig. 5 compares calculation results obtained with different approaches to a measurement result of axial magnetic flux density (B_z) along the magnet axis. The figure indicates total axial magnetic flux density with assuming that the operating current flows uniformly in each single pancake of the HTS magnet ($B_{z,Ideal}$), total axial magnetic flux density calculated by FEM ($B_{z,FEM}$), total axial magnetic flux density calculated with Bean slab model ($B_{z,Bean}$), and measured axial magnetic flux density ($B_{z,Measurement}$). Fig. 6 compares calculation and measurement results of SCF

Table II indicates results of comparison between Bean slab model and FEM in terms of computation time and accuracy; Analytic indicates results with Bean slab model, while Numerical with FEM. The accuracy is calculated by considering the mean value of the error, which is the most simple technique in error estimation discipline.

TABLE II
COMPUTATION TIME AND CALCULATION ACCURACY.

		Analytic	**Numerical**
Computation time	[sec]	500	7000
Computation accuracy	[%]	96	93

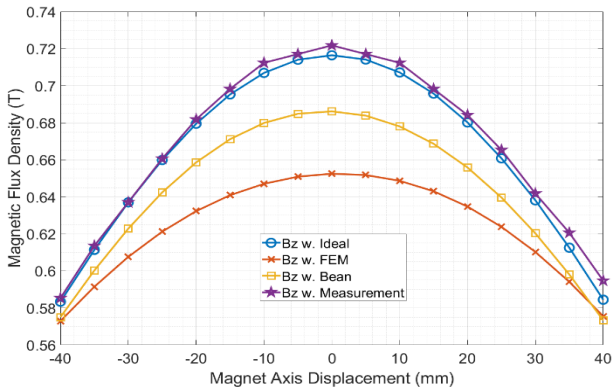

Fig. 5. Calculation and measurement results of total axial magnetic flux density.

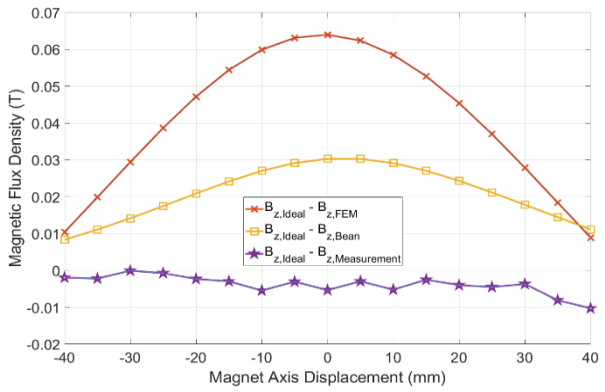

Fig. 6. Screening current induced field calculated by each approach and measured by MIT Francis Bitter Magnet Laboratory.

3.3. Discussion

The difference between simulation results of SCF was found. Because Bean slab model is known for extremely estimating or over-estimating screening current rather than other simulation approaches, such as FEM. However, Fig. 5 indicates the opposite result. To investigate the difference between the expectation and the calculation results, we examined radial component of total magnetic flux density and induced magnetic flux density by screening current, SCF. Fig. 7 shows simulation results: (a) total radial magnetic flux density assuming operating current flows uniformly in each single pancake of the HTS magnet ($B_{r_{tot,Ideal}}$); (b) total radial magnetic flux density with FEM ($B_{r_{tot,FEM}}$); (c) total radial magnetic flux density profile result with Bean slab model ($B_{r_{tot,Bean}}$); (d) radial component of SCF calculated by FEM ($B_{r_{sc,FEM}}$); and (e) radial component of SCF calculated by Bean slab model ($B_{r_{sc,Bean}}$). As shown in Fig. 7, calculated radial magnetic flux density with each simulation approach has a little discrepancy. A result of FEM shows that SCF is intensely induced around the center of each single pancake (SP). This result agrees with a conventional idea that SCF would eliminate radial magnetic field around the mid-plane of each SP. On the other hand, the calculated SCF with Bean slab model has a tendency that SCF is intensely induced at the edge side of SP, not the mid-plane. This tendency could cause the axial field to be calculated larger than that with

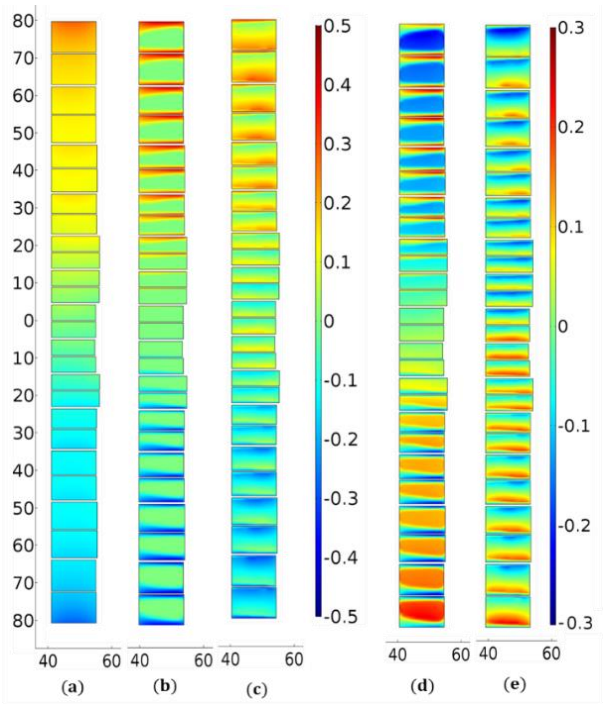

Fig. 7. Simulation results of the radial component of total magnetic flux density and SCF. (a) - (c) stand for total magnetic flux density, while (d) – (e) SCF. The y-axis indicates the DP z axis, while the x-axis is for the DP r axis in millimeters. Color bar indicates magnetic flux density in tesla T.

FEM; it might be a limit of Bean slab model calculating screening current without any iterative technique. To sum up, by this intrinsic difference between simulation approaches, comparison result from Table II may not be a determinant to evaluate which approach is although the comparison shows Bean slab model seems a better approach in terms of computation time and accuracy.

4. CONCLUSION

This paper presents simulation approaches, a case study indicating simulation results, and discussion. It reports that SCF degrades the magnetic field by 0.065 T (9%) with FEM, while 0.03 T (4%) with Bean slab model, where the degradation was calculated from the peak value of each approach compared with the measured data. This result might indicate the opposite against an expectation that the calculated SCF with Bean slab model is larger than that with FEM. Further, as seen in Fig. 6, the result with the ideal assumption, current flowing uniformly in an HTS magnet, has a good agreement with the measured data rather than that with other approaches. It implies that there are still a few things not considered yet, such as thermal contraction of an HTS tape in a cryogenic environment, lengthwise critical current data winding an HTS magnet, and other components affecting SCF. Thus it is required to conduct more studies with actually constructed HTS magnets in terms of SCF for developing far more precise simulation technique.

ACKNOWLEDGMENT

This work was supported by Research Resettlement Fund for the new faculty of Seoul National University.

REFERENCES

[1] S. G. Lee, S. Hahn, J. Kim, J. Y. Jang, Y. J. Hwan, J. Han, Y. Kim, H. Lee, S. H. In, H. K. Yeom, K. M. Kim, K. L. Kim, H. Yang and M. C. Ahn, "Development Progress of Metal-Clad No-Isulation All-REBCO Magnet for 400 MHz High Resolution NMR." Andong, *Korea: MEM 18*, 2018.

[2] J. Y. Jang, S. Yoon, S. Hahn, Y. J. Hwang, J. Kim, K. H. Shin, K. Cheon,Kim, S. In, Y.-J. Hong, H. Yeom, H. Lee, S.-H. Moon and S. Lee, "Design, construction and 13 K conduction-cooled operation of a 3 T 100 mm stainless steel cladding all-REBCO magnet," *Supercond. Sci. Technol*., vol. 30, no. 10, p. 105012, 2017.

[3] S. Hahn, J. Bascunan, H. Lee, E. S. Bobrov, W. Kim and Y. Iwasa, "Development of a 700 MHz low-/high-temperature superconductor for nuclear magnetic resonance magnet: Test results and spatial homogeneity improvement," *Rev. Sci. Instrum*., vol. 79, p. 023105, 2008.

[4] S. Hahn, J. Bascunan, H. Lee, E. S. Bobrov, W. Kim, M. C. Ahn and Y. Iwasa, "Operation and performance analyses of 350 and 700 MHz low-high-temperature superconductor nuclear magnetic resonance magnets A march toward operating frequencies above 1 GHz," *J. Appl. Phys*., vol. 105, no. 2, pp. 0245011-8, 2009.

[5] Y. Yanagisawa, H. Nakagome, K. Tennmei, M. Hamada, M. Yoshikawa, Otsuka, M. Hosono, T. Kiyoshi, M. Takahashi, T. Yamazaki and Maeda, "Operation of a 500 MHz high temperature superconducting NMR: Towards an NMR spectrometer operating beyond 1 GH," *J. Magn.Reson*., vol. 203, no. 2, pp. 274-282, 2010.

[6] T. Qu, P. C. Michael, J. Bascunan, T. Lecrevisse, M. Guan, S. Hahn and Y. Iwasa, "Test of an 8.66-T REBCO insert coil with overbanding radial build for a 1.3-GHz LTS/HTS NMR magnet," *IEEE Trans. Appl. Supercond*., vol. 27, no. 4, p. 4600605, 2017 and M. C. Ahn, T. Yagai, S. Hahn, R. Ando, J. Bascunan and Y. Iwasa, "Spatial and temporal variations of a screening current induced magnetic field in a double-pancake HTS insert of an LTS/HTS NMR magnet," *IEEE Trans. Appl. Supercond*., vol. 19, no. 3, pp. 4 301 205–2269– 4 301 205–2272, 2009.

[7] C. P. Bean, "Magnetization of high-field superconductors," *Rev. Mod. Phys*., vol. 36, pp. 31–39, 1964.

[8] E. H. Brandt and M. Indenbom, "Type-II-superconductor strip with current in a perpendicular magnetic field," *Phys. Rev. B*, vol. 48, no. 17, pp. 12893-12906, 1993.

[9] E. Zeldov, J. R. Clem, M. McElfresh and M. Darwin, "Magnetization and transport currents in thin superconducting films," *Phys. Rev. B*, vol. 49, no. 14, pp. 9802–9822, 1994.

[10] L. Wang, Q. Wang, J. Liu, H. Wang, X. Hu and P. Chen, "Screening current-induced magnetic field in a non-insulated GdBCO HTS coil for a 24 T all-superconducting magnet," *IEEE Trans. Appl. Supercond*., vol. 27, no. 4, p. 8200106, 2017.

[11] C. Navau, N. Del-Valle and A. Sanchez, "Macroscopic modeling of magnetization and levitation of hard type-II superconductors: The criticalstate model," *IEEE Trans. Appl. Supercond*., vol. 23, no. 1, p. 8201023, 2013.

[12] L. Prigozhin, "Analysis of critical-state problems in type-II superconduc-tivity," *IEEE Trans. Appl. Supercond*., vol. 7, no. 4, p. 3866-73, 1997.

[13] N. Amemiya, K. Miyamoto, S. Murasawa, H. Muka and K. Ohmatsu, "Finite element analysis of AC loss in non-twisted Bi-2223 tape carrying AC transport current and/or exposed to DC or AC external magnetic field," *Physica C*, vol. 310, pp. 30–35, 1998.

[14] G. Barnes, M. McCulloch and D. Dew-Hughes, "Computer modelling of type II superconductors in applications," *Supercond. Sci. Technol*., vol. 12, no. 8, pp. 518–522, 1999.

[15] S. Stavrev, F. Grilli, B. Dutoit, N. Nibbio, E. Vinot, I. Klutsch, G. Me-unier, P. Tixador, Y. Yang and E. Martines, "Comparison of numerical methods for modeling of superconductors," *IEEE Trans. Magn*., vol. 38, no. 2, pp. 849–52, 2002.

[16] N. Amemiya and K. Akachi, "Magnetic field generated by shielding current in high Tc superconducting coils for NMR magnets," *Supercond. Sci. Technol*., vol. 21, no. 9, p. 095001, 2008.

[17] M. A. Campbell, "A direct method for obtaining the critical state in two and three dimensions," *Supercond. Sci. Technol*., vol. 22, no. 3, p. 034005, Jan. 2009.

[18] H. Ueda, M. Fukuda, K. Hatanaka, K. Michitsuji, H. Karino, T. Wang, X. Wang, A. Ishiyama, S. Noguchi, Y. Yanagisawa and H. Maeda, "Measurement and simulation of magnetic field generated by screening currents in HTS coil," *IEEE Trans. Appl. Supercond*., vol. 24, no. 3, p. 4701505, 2014.

[19] H. Ueda, Y. Imaichi, T. Wang, A. Ishiyama, S. Noguchi, S. Iwai, H. Miyazaki, T. Tosaka, S. Nomura, T. Kurusu, S. Urayama and H. Fukuyama, "Numerical simulation on magnetic field generated by screening current in 10-T-class REBCO coil," *IEEE Trans. Appl. Supercond*., vol. 26, no. 4, p. 4701205, 2016.

[20] S. Kim, K. Sim, J. Cho, H.-M. Jang and M. Park, "AC loss analysis of HTS power cable with RABiTS coated conductor," *IEEE Trans. Appl. Supercond*., vol. 20, no. 3, pp. 2130–2133, 2010.

[21] D. N. Nguyen, S. P. Ashworth, J. O. Willis, F. Sirois and F. Grilli, "A new finite-element method simulation model for computing AC loss in roll assisted biaxially textured substrate YBCO tapes," *Supercond. Sci. Technol*., vol. 23, no. 2, p. 025001, 2009.

[22] M. Zhang and T. A. Coombs, "3D modelling of high- Tc superconductors by finite element software," *Supercond. Sci. Technol*., vol. 25, no. 1, p. 015009, 2011.

[23] F. Grilli, R. Brambilla, A. S. F. Sirois and S. Memiaghe, "Development of a three-dimensional finite-element model for high-temperature superconductors based on the H-formulation," *Cryogenics*, vol. 53, pp. 142–147, 2013.

[24] L. Queval, V. M. R. Zermeno and F. Grilli, "Numerical models for ac loss calculation in large-scale applications of HTS coated conductors," *Supercond. Sci. Technol*., vol. 29, no. 2, p. 024007, 2016.

[25] S. Kim, C. Lee and S. Hahn, "Manipulation of screening currents in an (RE)Ba2Cu3O7x Superconducting magnet," *Mater. Res. Express*, vol. 6, no. 2, pp. 0260041-8, 2018.

[26] S. Hahn, J. Song, Y. Kim, T. Lecrevisse, Y. Chu, J. Voccio, Bascunan and Y. Iwasa, "Construction and test of 7-T/68-mm cold-bore multiwidth no-insulation GdBCO magnet," *IEEE Trans. Appl. Supercond*., vol. 25, no. 3, p. 4600405, 2015.

[27] Y. J. Hwang, S. Hahn, S. G. Lee, J. Y. Jang, J. H. Han, H. Lee, J. Kim, H. Yeom, S. Yoon, K. Kim and M. C. Ahn, "A study on mitigation of screening current induced field with a 3 T 100 mm conduction-cooled metallic cladding REBCO magnet," *IEEE Trans. Appl. Supercond*., vol. 27, no. 4, p. 4701605, 2017.

[28] Y. Iwasa, Case Studies in Superconducting Magnets: Design and Operational Issues, New York, NY, USA: Springer-Verlag, 2009.

[29] V. M. R. Zermeno, A. B. Abrahamsen, N. Mijatovic, B. B. Jensen and M. P. Soerensen, "Calculation of AC losses in stacks and coils made of second generation high temperature superconducting tapes for large scale applications," *J. Appl. Phys*., vol. 114, no. 17, p. 173901, 2013.

[30] R. Brambilla, F. Grilli, L. Martini and F. Sirois, "Integral equations for the current density in thin conductors and their solution by the finite-element method," *Supercond. Sci. Technol*., vol. 21, no. 10, p. 10500, 2008.

[31] J. Rhyner, "Magnetic properties and AC-losses of superconductors with power-law current-voltage characteristics," *Physica C*, vol. 212, pp. 292-300, 1993.

[32] S. Wimbush and N. Strickland, "Critical current characterisation of SuNAM SAN04200 2G HTS superconducting wire," accessed 2017-07-07. [Online]. Available: https://doi.org/10.6084/m9.figshare.5182354.v1